Probing proton halo effects in the ⁸B+⁶⁴Zn collision around the Coulomb barrier

Downloaded from: https://research.chalmers.se, 2026-10-07 21:50 UTC

Citation for the original published paper (version of record):
Spartà, R., Di Pietro, A., Figuera, P. et al (2021). Probing proton halo effects in the ⁸B+⁶⁴Zn collision around the Coulomb barrier. Physics Letters, Section B: Nuclear, Elementary Particle and High-Energy Physics, 820. http://dx.doi.org/10.1016/j.physletb.2021.136477

N.B. When citing this work, cite the original published paper.

research.chalmers.se offers the possibility of retrieving research publications produced at Chalmers University of Technology. It covers all kind of research output: articles, dissertations, conference papers, reports etc. since 2004. research.chalmers.se is administrated and maintained by Chalmers Library

(article starts on next page)

Physics Letters B 820 (2021) 136477

Contents lists available at ScienceDirect

Physics Letters B

www.elsevier.com/locate/physletb

Probing proton halo effects in the ^{8}B+^{64}Zn collision around the Coulomb barrier

R. Spartà [a,b,*], A. Di Pietro [b], P. Figuera [b], O. Tengblad [c], A.M. Moro [d], I. Martel [e], J.P. Fernández-García [d,f], Jin Lei [g], L. Acosta [h,i], M.J.G. Borge [c], G. Bruni [j], J. Cederkäll [k], T. Davinson [l], J.D. Ovejas [c], L.M. Fraile [m,n], D. Galaviz [o], J. Halkjaer Jensen [p], B. Jonson [j], M. La Cognata [b], A. Perea [c], A.M. Sánchez-Benítez [e,q], N. Soić [r], S. Viñals [c]

[a] *Dipartamento di Fisica e Astronomia, Universitá di Catania, via S. Sofia 64, I-95123 Catania, Italy*
[b] *INFN, Laboratori Nazionali del Sud, via S. Sofia 62, 1-95123 Catania, Italy*
[c] *Instituto de Estructura de la Materia, CSIC, Serrano 113 bis, E-28006 Madrid, Spain*
[d] *Departamento de FAMN, Universidad de Sevilla, Apartado 1065, 41080 Sevilla, Spain*
[e] *Departamento de Física Aplicada, Universidad de Huelva, Campus de El Carmen, E-21071 Huelva, Spain*
[f] *Centro Nacional de Aceleradores, Universidad de Sevilla, Junta de Andalucía-CSIC, 41092 Sevilla, Spain*
[g] *INFN Sezione di Pisa, Largo Bruno Pontecorvo 3, 56127 Pisa, Italy*
[h] *Instituto de Física, Universidad Nacional Autónoma de México, A.P. 20-364, Mexico City 01000, Mexico*
[i] *INFN, Sezione di Catania, via S. Sofia 64, 1-95125 Catania, Italy*
[j] *Department of Physics, Chalmers University of Technology, S-41296 Göteborg, Sweden*
[k] *Physics Department, Lund University, Box 118, SE-221 00, Lund, Sweden*
[l] *School of Physics and Astronomy, University of Edinburgh, JCMB, Peter Guthrie Tait Road, Edinburgh EH9 3FD, United Kingdom of Great Britain and Northern Ireland*
[m] *Grupo de Física Nuclear & IPARCOS, Facultad de Ciencias Físicas, CEI Moncloa, 28040 Madrid, Spain*
[n] *ISOLDE, EP Department, CERN, CH-1211 Geneva-23, Switzerland*
[o] *LIP - Laboratory for Instrumentation and Experimental Particle Physics, Lisbon, Portugal*
[p] *Department of Physics and Astronomy, University of Aarhus, DK-8000 Aarhus, Denmark*
[q] *Centro de Estudios Avanzados en Física, Matemáticas y Computación (CEAFMC), Department of Integrated Sciences, University of Huelva, 21071 Huelva, Spain*
[r] *Ruđer Bošković Institute, Bijenička cesta, 54, HR-10000 Zagreb, Croatia*

ARTICLE INFO

Article history:
Received 1 April 2021
Received in revised form 31 May 2021
Accepted 23 June 2021
Available online 29 June 2021
Editor: B. Blank

Keywords:
Halo nuclei
Elastic scattering
Breakup

ABSTRACT

Proton halo effects in the ^{8}B+^{64}Zn reaction at an energy around 1.5 times the Coulomb barrier have been studied at HIE-ISOLDE CERN using, for the first time, the only existing postaccelerated ^{8}B beam. This, together with the use of a high granularity and large solid angle detection system, allowed for a careful mapping of the elastic angular distribution, especially in the Coulomb-nuclear interference region. Contrary to what is observed for the one-neutron halo nucleus ^{11}Be on the same target in a similar energy range, the analysis of the elastic scattering angular distribution shows only a modest suppression of the Coulomb-nuclear interference peak, with no remarkable enhancement of the total reaction cross-section. Inclusive angular and energy distributions of ^{7}Be produced in direct reaction processes have also been measured. The comparison of these data with the results of theoretical calculations for the elastic and non-elastic breakup contributions indicate that both processes are important. Overall, the experimental data suggest a ^{8}B collision dynamics at the barrier very different from the one of neutron halo nuclei, showing only modest effects of coupling to continuum. This behaviour can be interpreted as due to the presence of the additional Coulomb interactions halo-core and halo-target together with the presence of the centrifugal barrier felt by the valence proton of ^{8}B.

© 2021 The Authors. Published by Elsevier B.V. This is an open access article under the CC BY license (http://creativecommons.org/licenses/by/4.0/). Funded by SCOAP[3].

1. Introduction

The reaction dynamics around the Coulomb barrier (V_C) with halo nuclei has been extensively studied mainly for neutron halo (n-halo in the following) nuclei both from an experimental and

* Corresponding author at: Dipartamento di Fisica e Astronomia, Universitá di Catania, via S. Sofia 64, I-95123 Catania, Italy.
E-mail address: rsparta@lns.infn.it (R. Spartà).

https://doi.org/10.1016/j.physletb.2021.136477
0370-2693/© 2021 The Authors. Published by Elsevier B.V. This is an open access article under the CC BY license (http://creativecommons.org/licenses/by/4.0/). Funded by SCOAP[3].

theoretical point of view. Results can be summarised as follows. Close to the Coulomb barrier, coupling effects dominate the dynamics; since n-halo nuclei are extremely weakly bound, coupling to the continuum is known to be important. As a result of this coupling, elastic scattering angular distributions show a suppression in the Coulomb-nuclear interference region and considerable deviations from Rutherford scattering have been reported in the sub-barrier energy range e.g. [1–6]. A large total reaction cross-section σ_R is, as a consequence, observed. On heavy targets these results are mainly due to the coupling with the low-lying E1 strength in the continuum [1,3,6]. In the case of lighter targets, e.g. [5], nuclear as well as Coulomb coupling effects are important. For n-halo reactions a large fraction of the total reaction cross-section is due to direct processes such as breakup or transfer, e.g. [2,7–9].

First theoretical and experimental studies started to investigate whether similar effects are also present in the case of collisions induced by proton halo (p-halo in the following) nuclei around the barrier. The first published experimental data on this topic concerned reactions induced by ^{8}B. Indeed, this drip line nucleus is a good candidate for having a ground state p-halo structure because of its very low binding energy of 0.138 MeV against $^8\text{B}\rightarrow^7\text{Be+p}$ breakup. The existence of a p-halo in ^{8}B was suggested long ago (e.g. [10]) and, since then, has been widely debated in the literature. Recent results of various studies (see e.g. [11] and references therein) indicate the existence of an extended matter distribution in ^{8}B, in spite of the fact that the presence of the Coulomb and centrifugal barriers (being the valence proton in a p state) may inhibit the occurrence of the halo. Naively, due to the extremely low breakup threshold of ^{8}B, one might expect similar or even stronger effects than those observed in collisions involving n-halo nuclei.

Many of the investigations performed with ^{8}B beams concern Coulomb dissociation at energies well above the Coulomb barrier in order to get indirect information on the radiative capture reaction $^7\text{Be}(\text{p},\gamma)$ of astrophysical interest, e.g. [12–14]. Coulomb dissociation of p-halo nuclei shows a different behaviour from n-halo, in fact, the loosely bound valence proton actively participates in the reaction process. Contrary to the n-halo, in the case of p-halo the Coulomb interaction acts not only between the core and the target but also between the p and the core and the p and the target. Due to a dynamic polarization effect, the valence proton is expected to be displaced behind the nuclear core and shielded from the target (see e.g. [15,16]). In [17,18] it is shown how the interference between the various components of the Coulomb interaction is important in determining the outcome of the breakup process and how this interference depends on the energy and the Z of the target. In [17,19], the role of the p-core and p-target interaction in the p-halo breakup was studied theoretically. The effect of these additional potentials is to create an effective barrier, which makes the proton of the halo behave as if it was effectively more bound. Nuclear processes are expected also to have a primary role in the dissociation of ^{8}B [20,21].

There have been only a few experiments investigating the low energy reaction dynamics with p-halo nuclei (e.g. [22–30]). All experiments carried out so far have been done using in-flight produced ^{8}B beams, and therefore with the intrinsic limitations associated with the quality of such beams (purity, energy spread and beam emittance) compared to the postaccelerated ones.

Some of them show modest effects of the ^{8}B structure on the reaction dynamics. Firstly, in the elastic scattering angular distribution for the light system $^8\text{B+}^{12}\text{C}$ around the barrier [22] authors observe negligible continuum coupling effects and in the elastic scattering $^8\text{B+}^{27}\text{Al}$ measurement [23] a minor suppression of the Coulomb-nuclear interference peak is observed. A comparison of the deduced σ_R is often performed in this kind of analysis on a "reduced scale" to eliminate trivial static effects, i.e. those effects on the reaction cross-section simply due to the different Coulomb barriers and radii of the various systems which are being compared. In [23] σ_R is larger than the one induced by the well bound ^{16}O on the same target and in [22] this is confirmed while σ_R is found to be similar to that of weakly-bound nuclei on the same target. Likewise, modest effects of the ^{8}B structure were observed in the $^8\text{B+}^{208}\text{Pb}$ elastic scattering angular distribution measured at higher energies [24–26] (about 3 to 4 times the Coulomb barrier). Angular distributions in [25,26] and σ_R in [24,26] are qualitatively similar to those found for non-halo weakly-bound beams (e.g. $^6\text{Li},^7\text{Be}$) on the same target. Moreover, CDCC analysis of elastic angular distribution in [24–26] show only a small effect of coupling to the continuum. In [24,31] it is suggested that the high ^{8}B bombarding energy is not the reason why only a modest effect of coupling to continuum and a behaviour different from that of n-halo nuclei is observed. Indeed, CDCC calculations for collisions induced by ^{8}B and ^{11}Be on ^{208}Pb and ^{64}Zn, both close to the barrier and at about three times the barrier [24,31], show that the Coulomb and centrifugal barriers felt by the valence p in ^{8}B strongly suppress the coupling effects on the elastic channel and imply this very different behaviour between ^{8}B and n-halo nuclei scatterings.

Conversely, other experiments show important effects of the ^{8}B structure on the reaction dynamics. The $^8\text{B+}^{208}\text{Pb}$ elastic angular distribution close to the Coulomb barrier was recently reported in [27], where σ_R extracted via optical model (OM) fit was found to be much larger than in non halo weakly bound nuclei (^{7}Be, ^{6,7,8}Li) on the same target (comparing on a reduced scale). A similar situation is found in elastic scattering and breakup for $^8\text{B+}^{58}\text{Ni}$ which have been studied at various energies close to the barrier in [28,29]. The elastic angular distributions do not show a clear Coulomb-nuclear interference peak. The OM deduced σ_R was found to be similar than with n-halo beams, and larger than with stable weakly bound nuclei (Li and Be isotopes) on targets of similar mass.

In summary, a completely clear picture concerning dynamic effects in collisions around the Coulomb barrier induced by the p-halo ^{8}B has not yet emerged from the experimental data available in the literature. However, admittedly, the intrinsic characteristics of the in flight separated ^{8}B beams limited the quality of the experimental data with low angular resolution and a reduced number of data points in many of the measured angular distributions. The need for a complementary approach, by measuring the ^{8}B reaction at energies close to the Coulomb barrier with good energy and angular resolution, is obvious in order to have a clear understanding about the effects of ^{8}B structure on the reaction dynamics. To this aim we proposed to develop at HIE-ISOLDE CERN a postaccelerated ^{8}B beam with the goal to measure, using the large solid angle and high granularity detection system GLORIA, more precise angular distribution for elastic scattering and breakup on the medium mass target ^{64}Zn, that we have already used to perform extensive reaction dynamics studies at barrier energies using the n-halo nuclei ^{6}He [2,32,33], ^{11}Be [4,5] and, recently, ^{11}Li [34].

2. Experimental details

The experiment was performed at the HIE-ISOLDE facility of CERN [35] using for the first time a postaccelerated ^{8}B beam. ^{8}B was produced using protons of 1.4 GeV from the CERN PS Booster hitting a multiwalled carbon nanotube target (CNT). Molecules of $^8\text{BF}_2$ were extracted from the target and charge bred in REX electron beam ion source (EBIS) to the charge state 3^+. Finally, the ^{8}B was accelerated in the HIE-ISOLDE LINAC to an energy of 4.9 MeV/u. The beam was then transported to the multipurpose SEC scattering chamber where it impinged on a 1.02 mg/cm^2 ^{64}Zn target. The ^{64}Zn target was 98% isotopically enriched and manufactured at INFN-LNS. It was placed at an angle of 30° with respect to the beam direction, in order to allow measurements at 90°. The

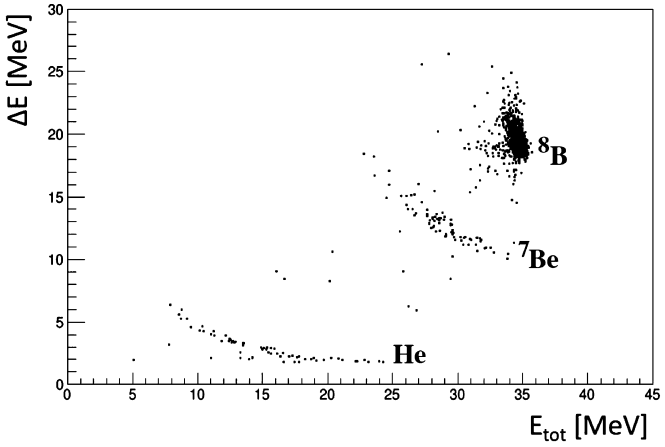

Fig. 1. ΔE *vs* total energy E_{tot} spectrum of telescope B ($15° \leq \theta \leq 62.5°$).

Table 1
Angular ranges covered by the six telescopes of the modified GLORIA array used in the present experiment.

Telescope	$\Delta\theta_{lab}$ [deg]
A	8.5-23
B	15-62.5
C = D	117-165
E	82-128
F	52-97.5

beam energy at the target center was 38.5 MeV. The final ^{8}B intensity on the reaction target was ∼400 pps. The beam intensity could not reach the maximum expected value of a few 10^3 pps due to the presence of an unforeseen $^{92}Mo^{2+}$ contaminant, having the same A/q, which was present in parts of the ion source [36]. Due to the high current of the contaminant, the full ^{8}B intensity extracted from the production target could not be cooled and bunched in the REXTRAP and was directly injected into EBIS, with a consequent loss in transmission of approximately one order of magnitude.

A silicon ΔE-E telescope was mounted downstream of the scattering chamber in order to monitor the purity and intensity of the ^{8}B beam. No evidence of contaminants was observed in the ^{8}B beam on target, after using a stripper foil placed before the last bending magnet of the SEC beam-line to eliminate contaminants.

The experimental setup was a modified version of the GLORIA [37] detector array, consisting in six silicon telescopes made of two stages of Si-detectors, 40 μm and 1000 μm thick respectively. Each detector was a 50x50 mm^2 Double Sided Silicon Strip Detector (DSSSD) segmented into 16+16 strips. This, combined with the small beam spot on target, of the order of 3 mm, allowed a high angular resolution measurement of the angular distribution. With respect to the standard GLORIA configuration [37], one of the two forward telescopes (telescope A) was moved farther from the target in order to cover angles down to θ_{lab}=8.5°. A ΔE-E plot from telescope B, is shown in Fig. 1. In the plot ^{8}B, ^{7}Be and He particles can be observed. These last ones may include unresolved ^{3}He and ^{4}He particles that can be produced in fusion-evaporation, incomplete fusion and ^{8}B breakup processes.

Table 1 gives the angular range covered by each telescope of the GLORIA array. The target to telescope distance was ∼15 cm for telescope A and ∼6 cm for all the other telescopes. Additional technical details of the GLORIA detector can be found in [37].

A crucial point of the data analysis is the proper reconstruction of the angle and solid angle values associated to each detector pixel. They were determined via a Monte Carlo simulation which made use not only of the known geometry of the set-up but also of the Rutherford scattering of a ^{12}C beam at 4.9 MeV/u onto a 300 μg/cm^2 thick Au target measured at HIE-ISOLDE CERN with the same experimental setup. As one can see in Fig. 2, the Rutherford shape of the elastic cross-section for $^{12}C+^{197}Au$ at 4.9 MeV/u is very well reproduced (mean deviation from Rutherford 1.8% in the angular range where ^{8}B data were analysed), giving confidence in the results from the analysis of the low intensity ^{8}B beam. The ∼5% deviation from Rutherford observed around 25° is due to a small difference between the ΔE and E angular coverage of the outer strips of detector B and was corrected for in the following ^{8}B analysis.

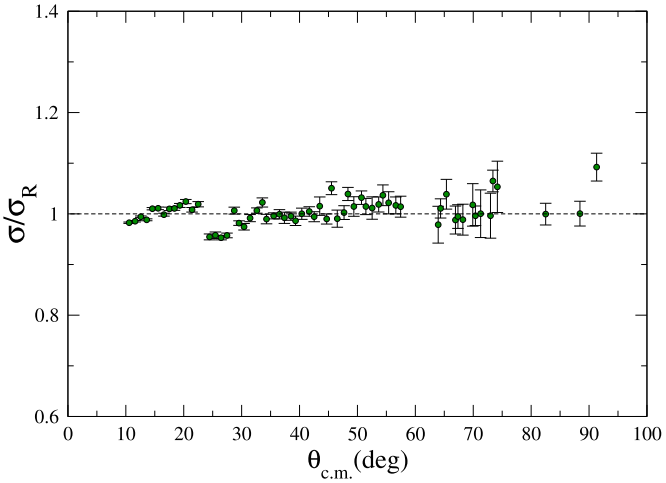

Fig. 2. Ratio of the experimental elastic scattering angular distribution for $^{12}C+^{197}Au$ at 4.9 MeV/u and the Rutherford cross-section.

3. Elastic scattering

Fig. 3 shows the $^{8}B+^{64}Zn$ elastic scattering angular distribution as a ratio to the Rutherford cross-section. It is worth noticing that the points corresponding to different detector telescopes fully overlap and a continuous angular distribution is obtained. Only data from telescopes A, B and F are shown due to lack of statistics at larger angles. The angular step is 1° for $\theta \leq 25°$, while for $\theta > 25°$ the angular step is 2°. The small angular step allowed the careful mapping of the Coulomb-nuclear interference region. It is worth recalling that the σ_R calculation from elastic scattering angular distributions is extremely sensitive to the data in this angular region. Contrary to the case of the n-halo nucleus ^{11}Be at similar $E_{c.m.}/V_C$ [4,5], a clear Coulomb-nuclear interference peak is visible at around 35°. The Coulomb barrier, calculated with the potential used in the following optical model analysis, is V_C=22.9 MeV.

The measured elastic data have been compared with continuum-discretized coupled-channels (CDCC) calculations at 38.5 MeV, in which the ^{8}B is described as a two-cluster system, ^{7}Be+p. The interaction between these two clusters is described with the effective potential containing central ($V_c(r)$) and spin-orbit ($V_{LS}(r)$ and $V_{LI}(r)$) components:

$$V(r) = V_c(r) + V_{LS}(r)\vec{\ell}\cdot\vec{s}_p + V_{LI}(r)\vec{\ell}\cdot\vec{I}, \quad (1)$$

where ℓ is the p-^{7}Be relative orbital angular momentum, $\vec{s}_p$ the proton spin and $\vec{I}$ the ^{7}Be spin. The same radial dependence was adopted for the three contributions, so that $V_x(r) = V_x^0 f(r, R_0, a_0)$, with $x = \{c, LS, LI\}$, V_x^0 is the potential strength and $f(r, R_0, a_0)$ the radial formfactor, which was assumed to follow the standard Woods-Saxon shape, with radius $R_0 = 2.391$ fm and diffuseness $a_0 = 0.535$ fm. The strengths of the spin-orbit terms were fixed

Table 2
Values (in MeV) of the depth of the central part of the p-^{7}Be potential adopted in the CDCC calculations. For other waves not listed in this Table, the model assumes the value for $J^\pi = 2^+$. See text for details.

J^π	2^+	1^+	0^+	3^+	1^-	2^-
V^0	44.70	45.05	42.46	33.07	55.18	63.46

to the values $V^0_{LS} = -8$ MeV and $V^0_{LI} = -2$ MeV. The depth of the central part is adjusted independently for each total angular momentum and parity of ^{8}B (J^π), so as to reproduce in the best possible way the known features of the ^{8}B low-lying spectrum. For the $J^\pi = 2^+$ states with $\ell = 1$, the strength was adjusted to give the ground-state separation energy. For $J^\pi = 1^+$ and $J = 3^+$ waves with $\ell = 1$, the depths were adjusted to reproduce the position of the well known resonances at $\varepsilon_{\rm res} = 0.63$ MeV and $\varepsilon_{\rm res} = 2.54$ MeV, respectively. For the $J^\pi = 0^+$ wave, the central depth was adjusted to reproduce the tentative resonance suggested in Ref. [38] at $\varepsilon_{\rm res} = 1.76$ MeV. Finally, for the $1^-, 2^-$ waves with $\ell = 0$ the strength was adjusted to reproduce the phase-shifts predicted by the ab-initio NCSMC calculation of Ref. [39] (see Table 2). For the remaining waves, the central depth was just kept equal to the value found for $J^\pi = 2^+$. In this model, the ground state wavefunction consists of a dominant $p_{3/2}$ configuration coupled to the ^{7}Be ground state, with a small admixture of the $p_{1/2}$ configuration. The ground state asymptotic normalization coefficient (ANC) squared is $C^2(p_{3/2}) + C^2(p_{1/2}) = 0.514$ fm^{-1}, which is consistent with the values extracted from different reactions [40–45] and microscopic calculations [46–48]. The ^{8}B continuum was discretized using the pseudostate (PS) method, in which the projectile Hamiltonian is diagonalized in a basis of square-integrable functions. For that purpose, in this work we use the Transformed Harmonic Oscillator (THO) basis obtained by application of a local scale transformation (LST) to the conventional HO basis. In particular, we used the analytical LST proposed in Refs. [49,50]. The range of the basis is controlled by the oscillator length (b) and the parameter γ (see Ref. [50] for details). We have used $b = 1.6$ fm and $\gamma = 2$ fm$^{-1/2}$. The size of the basis is determined by the number of oscillator functions (N), the maximum excitation energy ($\varepsilon_{\rm max}$) and the maximum orbital angular momentum for the core-valence motion ($\ell_{\rm max}$). In the present calculations we used $N = 15 - 20$, depending on the partial wave, $\varepsilon_{\rm max} = 12$ MeV and $\ell_{\rm max} = 3$. With these values of N, $\varepsilon_{\rm max}$ and $\ell_{\rm max}$, both the elastic and breakup observables are well converged. The CDCC calculations require also the proton-target and ^{7}Be-target optical potentials. For ^{7}Be + ^{64}Zn, we used the ^{7}Li optical potential of Cutler *et al.* [51], whereas for p + ^{64}Zn the systematic global potential of Koning and Delaroche [52] was adopted. The projectile-target coupling potentials were generated with the code THOx [53] and the coupled equations were solved with the code FRESCO [54].

The elastic differential cross-section obtained from these calculations is shown in Fig. 3a as a blue solid line. To highlight the effect of the ^{8}B elastic breakup on the elastic data, we include also the calculation omitting the coupling to the continuum channels (dashed line). By comparing these two calculations, one can see that the elastic breakup produces a small suppression of the elastic cross-section, which does not suppress completely the Coulomb-nuclear interference peak, as confirmed by the experimental data. CDCC calculations slightly underestimate the data at large angles. Effects not considered in the calculation, such as for example coupling to transfer, might be responsible for that.

The measured elastic scattering data have also been compared with Optical Model (OM) calculations. An analogous procedure to the one adopted in the ^{11}Be+^{64}Zn OM analysis [4] was used here. Since the scattering of the ^{7}Be core with the target was not measured, in the present case the ^{7}Li volume Woods-Saxon potential of Cutler *et al.* [51] was used, i.e. the same core-target potential

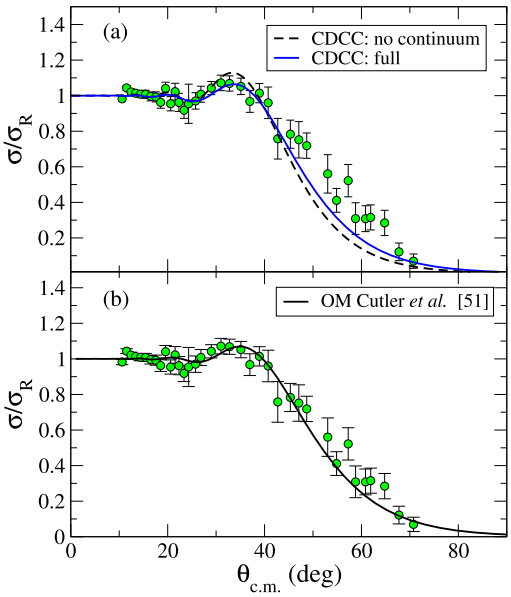

Fig. 3. Elastic scattering angular distribution for ^{8}B+^{64}Zn as a ratio to the Rutherford one (symbols). (a) Corresponding CDCC calculations with (full line) and without (dashed line) coupling to the continuum. (b) Optical model calculations using the potential parameters of [51] (full line).

adopted in the CDCC calculations. The potential has the following parameters: $V_0 = 220.4$ MeV, $r_0 = 0.798$ fm, for the real part, and $W_0 = 20.4$ MeV, $r_i = 1.164$ fm, for the imaginary part, and $a_r = a_i = 0.83$ fm. A standard Coulomb potential was added as well. The results are shown in Fig. 3(b). As one can see from the figure, the OM calculations with only the volume potential represent the angular distribution rather well particularly since they are not the result of a fit. Analogously to the procedure adopted in the study of ^{11}Be+^{64}Zn scattering [4] a fit was attempted by adding a surface potential to the volume term of [51], varying the three parameters of the surface component. However, in this case this fit did not improve the agreement with the data. In fact, the minimum χ^2 was obtained for a surface potential parameter depth $V_s \sim 0$. This result confirms the different behaviour between the p-halo ^{8}B and n-halo nuclei scattering. The present $\sigma_{\rm R}$ values for ^{8}B+^{64}Zn extracted both from CDCC ($\sigma_{\rm R}$ =1.5 b) and OM calculations ($\sigma_{\rm R}$ =1.3 b) are ≈50% smaller than those obtained with the n-halo ^{11}Be ($\sigma_{\rm R}$=2.7 b) on the same target and at similar $E_{\rm c.m.}/V_{\rm C}$, but comparable to that obtained in the reaction induced by the weakly bound ^{9}Be on ^{64}Zn (σ_R= 1.5 b) [4,5]. Fig. 4 shows the comparison of the ^{9,11}Be+^{64}Zn [4,5] and ^{8}B+^{64}Zn elastic scattering angular distributions at similar $E_{\rm c.m.}/V_{\rm C}$. From this qualitative comparison, one can clearly see that the ^{8}B angular distribution is similar to that of the weakly-bound ^{9}Be but differs significantly from that of the n-halo ^{11}Be, mainly in the Coulomb-nuclear interference region, indicating that ^{8}B does not show the strong effects of long-range absorption observed in the n-halo case. A possible explanation for this behaviour is discussed in [17,19]. In [17] it is shown that the single-particle wave function for the $p_{3/2}$ proton with respect to a ^{7}Be core with separation energy 0.14 MeV corresponds to that of a $p_{3/2}$ neutron with higher separation energy. The extra effective binding energy originates from the core-target Coulomb barrier. Moreover, the present experimental results are in agreement with the predictions of [31] where the authors perform CDCC calculations for ^{8}B+^{64}Zn at a laboratory energy of 32 MeV. Such calculations show only a modest suppression of the Coulomb-nuclear interference peak due to continuum coupling similar to the present case. However, it is shown that such suppression becomes large if one neglects in the calculations the Coulomb and

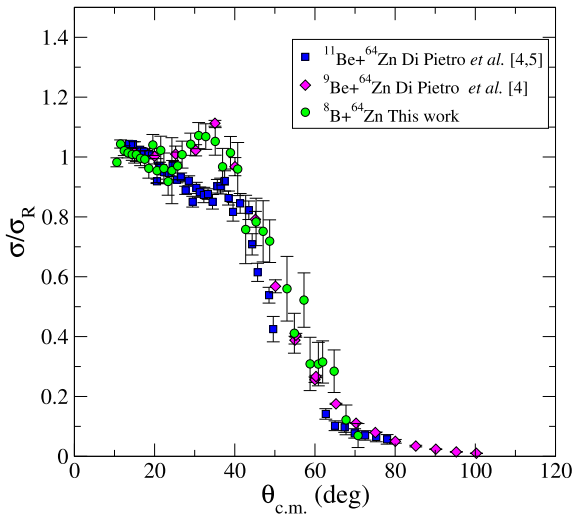

Fig. 4. Elastic scattering angular distribution of ^{8}B+^{64}Zn (green circles), ^{11}Be+^{64}Zn (blue squares), and ^{9}Be+^{64}Zn (magenta diamonds) as a ratio to the Rutherford cross-sections. The data of ^{9,11}Be+^{64}Zn are from [4,5].

centrifugal potentials felt by the valence proton, suggesting that the presence of such potentials generates a different behaviour between collisions induced by ^{8}B and n-halo nuclei in qualitative agreement with [17,19].

Instead, the present result appears to contradict what it was reported in [28] for a target of similar mass, were the ^{8}B+^{58}Ni elastic angular distribution was measured at 20 MeV< E_{lab} <30 MeV using an in-flight separated beam. The reaction cross-section was found to be enhanced with respect to the non-halo weakly bound nuclei and similar to that of n-halo induced reactions. The discrepancy of the present measurement and the one reported in [28] could be due to the small number of points and limited angular resolution of ^{8}B+^{58}Ni elastic scattering measurement. In fact, we remind that, in the case of strong absorption the total reaction cross-section is related to the difference between the Rutherford and the elastic cross-section [55]. Therefore, an accurate determination of the total reaction cross-section from the elastic scattering data, requires a detailed measurement of the angular distribution in the whole angular range but in particular in the Coulomb-nuclear interference region where the elastic cross-section deviates from Rutherford and is very large.

4. Breakup

In order to investigate the projectile breakup mechanism, the ^{7}Be angular and energy distributions were extracted from the data. The absolute normalisation of the cross-section was determined by normalising to Rutherford the elastic cross-section at $\theta_{c.m.} < 20°$. Fig. 5(a) shows the angular distribution for ^{7}Be events. As for the elastic scattering, data were gathered only from three out of six telescopes (detectors A, B and F) due to lack of statistics at backward angles. Since only the ^{7}Be fragments were measured, the present breakup data is inclusive, implying that several processes can in principle contribute to the ^{7}Be yield: on one side, the elastic breakup (EBU) process, in which the ^{8}B is dissociated into ^{7}Be+p, leaving the target in its ground state; on the other side, the nonelastic breakup (NEB) processes in which the dissociated proton interacts non-elastically with the target, including non-capture breakup accompanied by target excitation, proton absorption by the target (incomplete fusion) and proton transfer leading to bound states of ^{65}Cu. While the EBU contribution can be accurately computed with the CDCC method (described above), the evaluation of the NEB contribution is much more challenging due to the potentially large number of contributing processes. When one is only interested in the angular or energy distribution of the detected fragment (^{7}Be in our case) an efficient way of computing this NEB contribution is provided by the model of Ichimura, Austern and Vincent (IAV) [56]. Starting with the DWBA post-form amplitude and making use of the Feshbach projection formalism, the model provides a closed-form of the double differential cross-section of the detected fragments. The IAV model has been recently revisited by several groups [57–59] and its accuracy assessed against experimental data with considerable success [60,61]. The physical ingredients of the IAV model are similar to those of the CDCC calculations. Being based in the DWBA formalism, the IAV calculations require also the entrance channel optical potential. For that, we have used the potential of Cutler *et al.* [51] as in the CDCC and OM calculations.

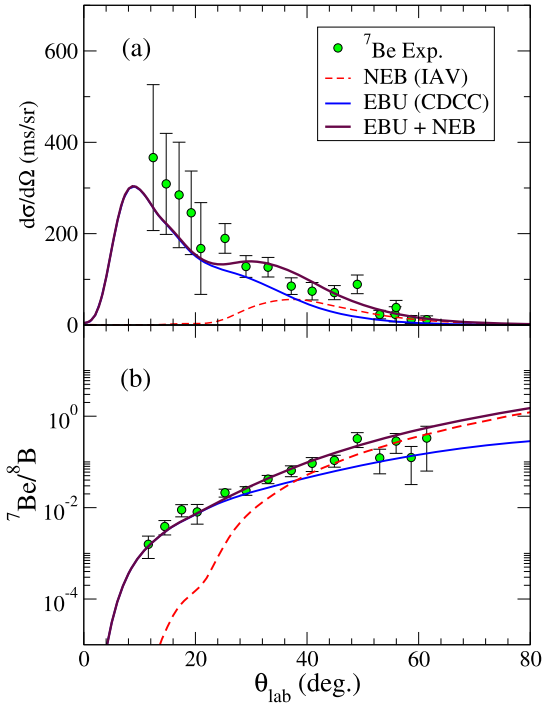

Fig. 5. a) ^{7}Be angular distribution and b) ^{7}Be breakup probability for the ^{8}B+^{64}Zn reaction. Symbols: experiment. Continuous blue line: EBU from CDCC calculations. Dashed red line: NEB. Continuous maroon line: sum of EBU+NEB contributions. See text for details.

In Fig. 5(a) the experimental ^{7}Be angular distribution is compared with the EBU and NEB calculations and their sum. The overall agreement between the experiment and the sum of EBU and NEB cross-section is fairly good, with only some underestimation of the data for θ_{lab} <20°. From this comparison it can be observed that the dominant reaction mechanism for the ^{7}Be production at forward angles is the EBU, although for θ_{lab} >30° the NEB contributions cannot be neglected. These results are in qualitative agreement with [26] for the ^{8}B+^{208}Pb reaction. Fig. 5(b) shows the breakup probability distribution, i.e. for a given angle the ratio of ^{7}Be events to elastic ^{8}B ones. Below θ_{lab} ≈40° EBU is larger than NEB while above the opposite is the case. From Fig. 5(b) it can be seen that the breakup probability is ∼30% (θ_{lab} ∼60°), ∼3% (θ_{lab} ∼30°) and ∼0.3% (θ_{lab} ∼15°). The calculated cross-sections associated with the EBU and NEB are, respectively, σ_{EBU} =215 mb and σ_{NEB} =100 mb corresponding to a EBU+NEB cross-section which is of the order of 20-25% of σ_R. This result is considerably lower than that observed in the collisions induced by the n-halo nuclei ^{11}Be and ^{6}He on the same target at a similar

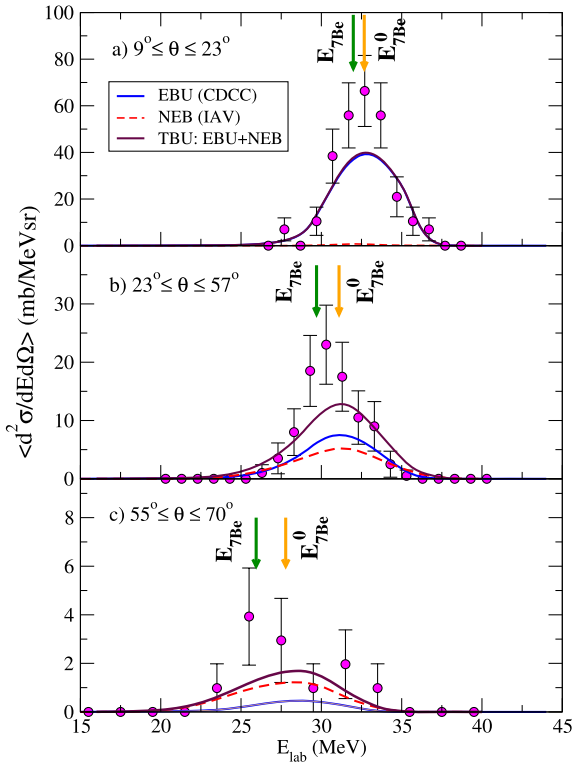

Fig. 6. ^{7}Be energy distribution averaged over the solid angle of the detector covering the angular range indicated for a) detector A, b) detector B and c) detector F. The continuous blue line, dashed red line and continuous brown lines are for the EBU, NEB calculations and their sum, respectively. The orange and green arrows are the classical kinematical estimates for the asymptotic and near-target breakup scenarios, respectively. As discussed in the text, a conclusion on near-target or asymptotic breakup cannot be drawn from this simple comparison.

$E_{\mathrm{c.m.}}/V_{\mathrm{C}}$, where the ratio $\sigma_{\mathrm{breakup}}/\sigma_{\mathrm{R}}$ was respectively 40% [4] and 70% [33].

Fig. 6 shows the energy distribution of ^{7}Be events averaged over the corresponding solid angle (Top panel: $9° < \theta_{\mathrm{lab}} < 23°$ telescope A. Middle panel: $23° < \theta_{\mathrm{lab}} < 57°$ telescope B. Bottom panel: $55° < \theta_{\mathrm{lab}} < 70°$ telescope F) and corrected for the energy loss in the target and detector dead-layers. The energy distribution is rather well reproduced by the sum of the corresponding EBU and NEB calculations, confirming the underestimation observed at the smallest angles in the angular distribution. The experimental width and centroid of the distribution, within the associated errors, is also very well described by the theory. The importance of taking into consideration both EBU and NEB processes is apparent also from this comparison.

As emphasized by previous works [62–66], the position of the peak of the energy distribution may provide information on the reaction dynamics. For that, one could try to compare this position with simple kinematical estimates based on classical considerations. In particular, we consider two such estimates. In the first one, we assume that the projectile dissociation takes place far from the target, asymptotically. Under this situation, one expects that the total kinetic energy carried by the ^{8}B system will be distributed among the proton and ^{7}Be fragments proportionally to their masses. Then, the ^{7}Be would be detected at an energy of approximately 7/8 of the kinetic energy of ^{8}B* (mean ^{8}B excitation energy estimated from CDCC calculations), that we denote $E^{0}_{^{7}\mathrm{Be}}(\theta)$). This is indicated by the orange arrows in Fig. 6. It is important to notice that the definition of $E^{0}_{^{7}\mathrm{Be}}(\theta)$ is not unique in the literature since in some cases this is considered as 7/8 of the elastic scattering ^{8}B energy (e.g. [67]). In the second estimate, conversely, we assume instead that breakup takes place near the target nucleus, where part of the projectile kinetic energy has been transformed into Coulomb potential energy. After the projectile dissociates into ^{7}Be+p, this Coulomb energy will be converted into kinetic energy and distributed among the fragments according to their charges. Denoting the breakup distance by R_{bu} (approximated as the distance of closest approach in a classical Coulomb trajectory) the ^{7}Be would be observed with an energy [68]

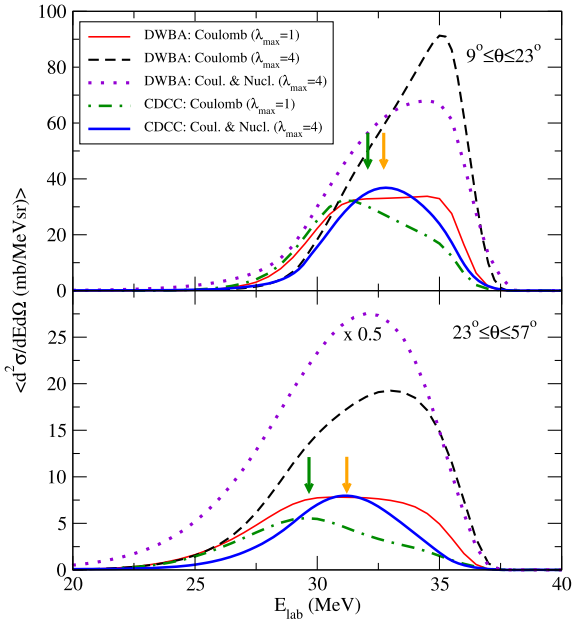

Fig. 7. Calculated ^{7}Be energy distribution in the angular range $9° \leq \theta \leq 23°$ (top) and $23° \leq \theta \leq 57°$ (bottom). DWBA calculations: only Coulomb E1 breakup (thin red line); Coulomb breakup with higher multipolarities (λ_{max}=4) (dashed black line) and Coulomb+nuclear breakup (dotted violet line). CDCC calculations: only Coulomb E1 breakup (dot-dashed green line) and Coulomb+nuclear breakup (thick blue line). The orange and green arrows are the classical kinematical estimates for the asymptotic and near-target breakup scenarios, respectively. See text for details.

$$E_{^{7}\mathrm{Be}}(\theta) = E^{0}_{^{7}\mathrm{Be}}(\theta) + \frac{Z_p Z_t e^2}{R_{\mathrm{bu}}}\left[\frac{Z_c m_p - m_c Z_p}{Z_p m_p}\right] \quad (2)$$

where $Z_{p,c,t}$ are the projectile, core and target charges, respectively and $m_{p,c}$ the projectile and core masses. The first term on the right hand side of this equation is just the asymptotic estimate, whereas the second term is due to the Coulomb postacceleration effect described above. In Fig. 6, the orange and green arrows correspond to the asymptotic ($E^{0}_{^{7}\mathrm{Be}}$) and near-target breakup ($E_{^{7}\mathrm{Be}}$) estimates. It is seen that the estimated energy shift is negative in this case, so it would actually results in a deceleration of the ^{7}Be with respect to the asymptotic breakup scenario. Furthermore, it is seen that the experimental energy peak is closer to the estimate excluding postacceleration. At first sight, this might suggest an asymptotic breakup scenario. However, this is not necessarily the case, since, as it will be discussed in the following, there are other effects which affect the ^{7}Be energy distribution. Indeed, as discussed in the introduction, the breakup dynamics in the case of ^{8}B is rather complex. Therefore, particular care must be taken before drawing any conclusion on asymptotic or near-target breakup just by comparing the energy distribution of the breakup fragments with simple classical estimates. In order to gain further insight into breakup dynamics and postacceleration effects full CDCC calculations, where the postacceleration effect is accounted by the continuum-continuum couplings, were compared with DWBA calculations, where the coupling to the continuum is treated to first order and thus it does not account for the postacceleration. Fig. 7

shows, as an example, the calculated ^{7}Be energy distributions in the angular ranges $9^\circ \leq \theta \leq 23^\circ$ and $23^\circ \leq \theta \leq 57^\circ$. The thin red line represents DWBA calculations where only the Coulomb dipole contribution E1 is considered. The distribution has a flat top with its centroid compatible with the classical estimate for no postacceleration (orange arrow). However, as shown in e.g. [16,18,69], the shape of the ^{7}Be energy distribution is affected by the interference between E1 and E2 (and higher) multipoles. When these additional couplings are added (dashed black line) the maximum of the distribution is shifted towards higher energies. The inclusion of the nuclear breakup, still in first order, (dotted violet line) shifts the maximum to energies lower than considering only Coulomb contribution. The situation changes when these couplings are consider beyond the first order. For example, the CDCC calculation including only E1 couplings to all orders (dot-dashed green line) predicts an energy distribution displaying deceleration effect, with a centroid very close to the near-target breakup estimate (green arrow). However, when higher multipolarities and nuclear couplings are included in the CDCC calculations (thick blue-line), the maximum is shifted back to a position very close to the classical estimate without postacceleration.

From these test calculations, the following conclusions can be drawn. (i) The comparison of first order (DWBA) with all-orders (CDCC) calculations including only E1 Coulomb couplings confirms the expected deceleration effect predicted by the classical model, thus suggesting a near-target breakup scenario; (ii) however, this picture breaks down when higher Coulomb multipoles, as well as nuclear couplings, are considered. In particular, the full CDCC calculations display no apparent acceleration or deceleration of the ^{7}Be fragment with respect to the ^{8}B c.m. motion. These results evidence that the dynamics of the ^{8}B breakup is much more complicated than suggested by the simple classical picture outlined above. This is at variance with the case of the n-halo nucleus ^{11}Be, where similar classical estimates proved very successfully at describing the ^{10}Be energy following breakup [65,66]. The ^{8}B behaviour can be interpreted (see e.g. [17,19,31]) as due to the presence of the additional Coulomb interactions halo-core and halo-target together with the presence of the centrifugal barrier experienced by the valence proton of ^{8}B.

5. Summary and conclusions

The use of a high-quality postaccelerated beam combined with GLORIA, a high granularity and large solid angle detection setup, allowed for the measurement around the Coulomb barrier energy of a detailed ^{8}B+^{64}Zn elastic angular distribution, where the Coulomb-nuclear interference region is carefully mapped. The comparison with CDCC calculations disclosed the evidence that reaction dynamics for the p-halo ^{8}B shows only modest effects of coupling to the continuum and its σ_R is similar to that of ordinary weakly bound nuclei on the same target.

The inclusive angular and energy ^{7}Be distributions have been provided, distinctively showing a dominance of elastic breakup at small angles, whereas non-elastic breakup becomes non negligible at larger angles. The total breakup cross-section is of the order of 20-25% of σ_R, suggesting once more a different behaviour between the p-halo ^{8}B and n-halo nuclei.

CDCC and DWBA calculations have shown that the ^{7}Be energy distribution is determined by various effects, most notably the contribution of different Coulomb multipoles in the breakup process and their interference, as well as nuclear effects. Restricted CDCC calculations, including only E1 Coulomb couplings, suggest a near-target breakup scenario. However, the comparison with the full CDCC calculations indicates that this does not lead to an energy shift of the outgoing ^{7}Be fragments, as predicted by the simple classical model, due to the interplay of other dynamical effects.

In conclusion, in spite of the extremely low ^{8}B breakup threshold and its extended nuclear matter density distribution [11], the present experimental results clearly show that the ^{8}B reaction dynamics is very different from that of n-halo nuclei.

This complex scenario clearly shows that a proper understanding of the dynamics of proton-halo nuclei, including the role of postacceleration and the dependence of the relative contribution of elastic and non elastic breakup on the target, calls for further investigations. All these effects can be better elucidated by additional ^{8}B breakup experimental studies, specifically those including exclusive measurements of all outgoing fragments.

Declaration of competing interest

The authors declare that they have no known competing financial interests or personal relationships that could have appeared to influence the work reported in this paper.

Acknowledgements

We wish to thank Dr. A. Bonaccorso for useful discussions and suggestions. This work has been supported by the European Commission Horizon 2020 framework trans-national access program of the EU project ENSAR2 (Grant no. 654002). Some of us acknowledge the support of the Istituto Nazionale di Fisica Nucleare (INFN), the UKRI STFC and the Spanish Funding Agency under the projects: "ELEGANT" PGC2018-095640-B-100, FIS2017-88410-P, PDI2019-104390GB-100, FPA2016-77689-C2-1-R, PGC2018-096994-B-C21, PGC2018-096994-B-C22, RTI2018-098868-B-I00. L.A. is partially supported by DGAPA PAPIIT-IN107820 and CONACYT 314857. L.M.F is partially supported by the CERN associates program. D.G. is supported by the Portuguese FCT under the project CERN/FIS-PAR/0005/2017.

References

[1] A. Sánchez-Benítez, et al., Study of the elastic scattering of ^{6}He on ^{208}Pb at energies around the Coulomb barrier, Nucl. Phys. A 803 (1) (2008) 30–45, https://doi.org/10.1016/j.nuclphysa.2008.01.030.

[2] A. Di Pietro, et al., Reactions induced by the halo nucleus ^{6}He at energies around the Coulomb barrier, Phys. Rev. C 69 (2004) 044613, https://doi.org/10.1103/PhysRevC.69.044613.

[3] M. Cubero, et al., Do halo nuclei follow Rutherford elastic scattering at energies below the barrier? The case of ^{11}Li, Phys. Rev. Lett. 109 (2012) 262701, https://doi.org/10.1103/PhysRevLett.109.262701.

[4] A. Di Pietro, et al., Elastic scattering and reaction mechanisms of the halo nucleus ^{11}Be around the Coulomb Barrier, Phys. Rev. Lett. 105 (2010) 022701, https://doi.org/10.1103/PhysRevLett.105.022701.

[5] A. Di Pietro, et al., Experimental study of the collision ^{11}Be + ^{64}Zn around the Coulomb barrier, Phys. Rev. C 85 (2012) 054607, https://doi.org/10.1103/PhysRevC.85.054607.

[6] V. Pesudo, et al., Scattering of the halo nucleus ^{11}Be on ^{197}Au at energies around the Coulomb barrier, Phys. Rev. Lett. 118 (2017) 152502, https://doi.org/10.1103/PhysRevLett.118.152502.

[7] R. Raabe, et al., No enhancement of fusion probability by the neutron halo of ^{6}He, Nature 431 (2004) 823–826, https://doi.org/10.1038/nature02984.

[8] J. Fernández-García, et al., ^{11}Li breakup on ^{208}Pb at energies around the Coulomb Barrier, Phys. Rev. Lett. 110 (2013) 142701, https://doi.org/10.1103/PhysRevLett.110.142701.

[9] A. Chatterjee, et al., 1n and 2n transfer with the Borromean nucleus ^{6}He near the Coulomb barrier, Phys. Rev. Lett. 101 (2008) 032701, https://doi.org/10.1103/PhysRevLett.101.032701.

[10] T. Minimasono, Proton halo of ^{8}B disclosed by its giant quadrupole moment, Phys. Rev. Lett. 69 (1992) 2058–2061, https://doi.org/10.1103/PhysRevLett.69.2058.

[11] A. Dobrovolsky, et al., Nuclear-matter distribution in the proton-rich nuclei ^{7}Be and ^{8}B from intermediate energy proton elastic scattering in inverse kinematics, Nucl. Phys. A 989 (2019) 40–58, https://doi.org/10.1016/j.nuclphysa.2019.05.012.

[12] N. Iwasa, et al., Study of the ^{7}Be(p, γ) ^{8}B reaction with the Coulomb dissociation method, J. Phys. Soc. Jpn. 65 (5) (1996) 1256–1263, https://doi.org/10.1143/JPSJ.65.1256.

[13] B. Davids, S.M. Austin, D. Bazin, H. Esbensen, B.M. Sherrill, I.J. Thompson, J.A. Tostevin, Electromagnetic dissociation of ^{8}B and the rate of the ^{7}Be$(p,\gamma)^{8}$B reaction in the sun, Phys. Rev. C 63 (2001) 065806, https://doi.org/10.1103/PhysRevC.63.065806.

[14] F. Schümann, et al., Coulomb dissociation of ^{8}B and the low-energy cross section of the ^{7}Be$(p,\gamma)^{8}$B solar fusion reaction, Phys. Rev. Lett. 90 (2003) 232501, https://doi.org/10.1103/PhysRevLett.90.232501.

[15] A. García-Camacho, G. Blanchon, A. Bonaccorso, D.M. Brink, All orders proton breakup from exotic nuclei, Phys. Rev. C 76 (2007) 014607, https://doi.org/10.1103/PhysRevC.76.014607.

[16] J.F. Liang, et al., Dynamic polarization in the coulomb breakup of loosely bound ^{17}f, Phys. Lett. B 681 (2009) 22, https://doi.org/10.1016/j.physletb.2009.09.055.

[17] R. Kumar, A. Bonaccorso, Dynamical effects in proton breakup from exotic nuclei, Phys. Rev. C 84 (2011) 014613, https://doi.org/10.1103/PhysRevC.84.014613.

[18] R. Kumar, A. Bonaccorso, Interplay of nuclear and Coulomb effects in proton breakup from exotic nuclei, Phys. Rev. C 86 (2012) 061601(R), https://doi.org/10.1103/PhysRevC.86.061601.

[19] A. Bonaccorso, D.M. Brink, C.A. Bertulani, Proton vs neutron halo breakup, Phys. Rev. C 69 (2004) 024615, https://doi.org/10.1103/PhysRevC.69.024615.

[20] C. Dasso, S. Lenzi, A. Vitturi, Dominance of nuclear processes in the dissociation of ^{8}B, Nucl. Phys. A 639 (3) (1998) 635–653, https://doi.org/10.1016/S0375-9474(98)00420-5.

[21] B. Blank, et al., Total interaction and proton-removal cross-section measurements for the proton-rich isotopes ^{7}Be, ^{8}B, and ^{9}C, Nucl. Phys. A 624 (2) (1997) 242–256, https://doi.org/10.1016/S0375-9474(97)81837-4.

[22] A. Barioni, et al., Elastic scattering and total reaction cross sections for the ^{8}B, ^{7}Be, and ^{6}Li + ^{12}C systems, Phys. Rev. C 84 (2011) 014603, https://doi.org/10.1103/PhysRevC.84.014603.

[23] V. Morcelle, et al., ^{8}B +^{27} Al scattering at low energies, Phys. Rev. C 95 (2017) 014615, https://doi.org/10.1103/PhysRevC.95.014615.

[24] Y.Y. Yang, et al., Elastic scattering of the proton drip line nuclei ^{7}Be,^{8} B, and ^{9}C on a lead target at energies around three times the coulomb barriers, Phys. Rev. C 98 (2018) 044608, https://doi.org/10.1103/PhysRevC.98.044608.

[25] Y. Yang, et al., Elastic scattering of the proton drip-line nucleus ^{8}B off a $^{\text{nat}}$Pb target at 170.3 MeV, Phys. Rev. C 87 (2013) 044613, https://doi.org/10.1103/PhysRevC.87.044613.

[26] K. Wang, et al., Elastic scattering and breakup reactions of the proton drip-line nucleus ^{8}B on ^{208}Pb at 238 MeV, Phys. Rev. C 103 (2021) 024606, https://doi.org/10.1103/PhysRevC.103.024606.

[27] M. Mazzocco, et al., Elastic scattering for the ^{8}B and ^{7}Be +^{208} Pb systems at near-Coulomb barrier energies, Phys. Rev. C 100 (2019) 024602, https://doi.org/10.1103/PhysRevC.100.024602.

[28] E. Aguilera, et al., Reaction cross sections for ^{8}B, ^{7}Be, and ^{6}Li +^{58} Ni near the coulomb barrier: proton-halo effects, Phys. Rev. C 79 (2009) 021601, https://doi.org/10.1103/PhysRevC.79.021601.

[29] V. Guimarães, et al., Nuclear and Coulomb interaction in ^{8}B breakup at sub-Coulomb energies, Phys. Rev. Lett. 84 (2000) 1862–1865, https://doi.org/10.1103/PhysRevLett.84.1862.

[30] A. Pakou, et al., Dominance of direct reaction channels at deep sub-barrier energies for weakly bound nuclei on heavy targets: the case ^{8}B +^{208} Pb, Phys. Rev. C 102 (2020) 031601, https://doi.org/10.1103/PhysRevC.102.031601.

[31] Y.Y. Yang, X. Liu, D.Y. Pang, Distinction between elastic scattering of weakly bound proton- and neutron-rich nuclei: the case of ^{8}B and ^{11}Be, Phys. Rev. C 94 (2016) 034614, https://doi.org/10.1103/PhysRevC.94.034614.

[32] V. Scuderi, et al., Fusion and direct reactions for the system ^{6}He + ^{64}Zn at and below the Coulomb barrier, Phys. Rev. C 84 (2011) 064604, https://doi.org/10.1103/PhysRevC.84.064604.

[33] J.P. Fernández-García, A. Di Pietro, P. Figuera, J. Gómez-Camacho, M. Lattuada, J. Lei, A.M. Moro, M. Rodríguez-Gallardo, V. Scuderi, Breakup mechanisms in the ^{6}He +^{64} Zn reaction at near-barrier energies, Phys. Rev. C 99 (2019) 054605, https://doi.org/10.1103/PhysRevC.99.054605.

[34] J.P. Fernández-García, et al., to be published.

[35] Y. Kadi, Y. Blumenfeld, W.V. Delsolaro, M.A. Fraser, M. Huyse, A.P. Koufidou, J.A. Rodriguez, F. Wenander, Post-accelerated beams at ISOLDE, J. Phys. G, Nucl. Part. Phys. 44 (8) (2017) 084003, https://doi.org/10.1088/1361-6471/aa78ca.

[36] J. Ballof, et al., Radioactive boron beams produced by isotope online mass separation at CERN-ISOLDE, Eur. Phys. J. A 55 (5) (2019) 65, https://doi.org/10.1140/epja/i2019-12719-1.

[37] G. Marquínez-Durán, L. Acosta, R. Berjillos, J. Dueñas, J. Labrador, K. Rusek, A. Sánchez-Benítez, I. Martel, GLORIA: a compact detector system for studying heavy ion reactions using radioactive beams, Nucl. Instrum. Methods Phys. Res., Sect. A 755 (2014) 69–77, https://doi.org/10.1016/j.nima.2014.04.002.

[38] J. Mitchell, et al., Structure of ^{8}B from elastic and inelastic ^{7}Be+p scattering, Phys. Rev. C 87 (2013) 054617, https://doi.org/10.1103/PhysRevC.87.054617.

[39] P. Navrátil, R. Roth, S. Quaglioni, Ab initio many-body calculation of the ^{7}Be(p,γ)^{8}B radiative capture, Phys. Lett. B 704 (5) (2011) 379–383, https://doi.org/10.1016/j.physletb.2011.09.079.

[40] L. Trache, F. Carstoiu, C.A. Gagliardi, R.E. Tribble, Asymptotic normalization coefficient of ^{8}B from breakup reactions and the s_{17} astrophysical factor, Phys. Rev. Lett. 87 (2001) 271102, https://doi.org/10.1103/PhysRevLett.87.271102.

[41] K. Ogata, S. Hashimoto, Y. Iseri, M. Kamimura, M. Yahiro, Determination of S_{17} from ^{8}B breakup by means of the method of continuum-discretized coupled channels, Phys. Rev. C 73 (2006) 024605, https://doi.org/10.1103/PhysRevC.73.024605.

[42] G. Tabacaru, et al., Scattering of ^{7}Be and ^{8}B and the astrophysical s_{17} factor, Phys. Rev. C 73 (2006) 025808, https://doi.org/10.1103/PhysRevC.73.025808.

[43] S.B. Igamov, R. Yarmukhamedov, Asymptotic normalization coefficients (nuclear vertex constants) for p+^{7}Be $\rightarrow$ ^{8}B and the direct ^{7}Be(p,γ)^{8}B astrophysical S factors at solar energies, Phys. At. Nucl. 71 (2008) 1740, https://doi.org/10.1134/S1063778808100098.

[44] T.L. Belyaeva, E.F. Aguilera, E. Martinez-Quiroz, A.M. Moro, J.J. Kolata, Astrophysical $S_{17}(0)$ factor extraction from breakup of ^{8}B on ^{58}Ni at energies near the Coulomb barrier, Phys. Rev. C 80 (2009) 064617, https://doi.org/10.1103/PhysRevC.80.064617.

[45] O.R. Tojiboev, R. Yarmukhamedov, S.V. Artemov, S.B. Sakuta, Asymptotic normalization coefficients for ^{7}Be + $p \rightarrow^{8}$ B from the peripheral ^{7}Be$(d,n)^{8}$B reaction and their astrophysical application, Phys. Rev. C 94 (2016) 054616, https://doi.org/10.1103/PhysRevC.94.054616.

[46] P. Descouvemont, Reanalysis of the ^{7}Be$(p,\gamma)^{8}$B s factor in a microscopic model, Phys. Rev. C 70 (2004) 065802, https://doi.org/10.1103/PhysRevC.70.065802.

[47] J. Huang, C. Bertulani, V. Guimarães, Radiative capture of nucleons at astrophysical energies with single-particle states, At. Data Nucl. Data Tables 96 (6) (2010) 824–847, https://doi.org/10.1016/j.adt.2010.06.004.

[48] K.M. Nollett, R.B. Wiringa, Asymptotic normalization coefficients from ab initio calculations, Phys. Rev. C 83 (2011) 041001, https://doi.org/10.1103/PhysRevC.83.041001.

[49] S. Karataglidis, K. Amos, B.G. Giraud, Local scale transformations and extended matter distributions in nuclei, Phys. Rev. C 71 (2005) 064601, https://doi.org/10.1103/PhysRevC.71.064601.

[50] J.A. Lay, A.M. Moro, J.M. Arias, J. Gómez-Camacho, Particle motion in a deformed potential using a transformed oscillator basis, Phys. Rev. C 85 (2012) 054618, https://doi.org/10.1103/PhysRevC.85.054618.

[51] R. Cutler, M. Nadworny, K. Kemper, 28-and 34-MeV Li6 and Li7 elastic scattering on nuclei with $40 \leq a \leq 91$, Phys. Rev. C 15 (4) (1977) 1318.

[52] A. Koning, J. Delaroche, Local and global nucleon optical models from 1 keV to 200 MeV, Nucl. Phys. A 713 (3) (2003) 231–310, https://doi.org/10.1016/S0375-9474(02)01321-0.

[53] R. de Diego, J.M. Arias, J.A. Lay, A.M. Moro, Phys. Rev. C 89 (6) (2014) 064609, https://doi.org/10.1103/PhysRevC.89.064609.

[54] I.J. Thompson, Coupled reaction channels calculations in nuclear physics, Comput. Phys. Rep. 7 (4) (1988) 167–212, https://doi.org/10.1016/0167-7977(88)90005-6.

[55] G.R. Satchler, Introduction to Nuclear Reactions, Macmillan Education LTD, 1990.

[56] M. Ichimura, N. Austern, C.M. Vincent, Equivalence of post and prior sum rules for inclusive breakup reactions, Phys. Rev. C 32 (1985) 431–439, https://doi.org/10.1103/PhysRevC.32.431.

[57] B.V. Carlson, R. Capote, M. Sin, Inclusive proton emission spectra from deuteron breakup reactions, Few-Body Syst. 57 (5) (2016) 307–314, https://doi.org/10.1007/s00601-016-1054-8.

[58] J. Lei, A.M. Moro, Reexamining closed-form formulae for inclusive breakup: application to deuteron- and ^{6}Li-induced reactions, Phys. Rev. C 92 (2015) 044616, https://doi.org/10.1103/PhysRevC.92.044616.

[59] G. Potel, F.M. Nunes, I.J. Thompson, Establishing a theory for deuteron-induced surrogate reactions, Phys. Rev. C 92 (2015) 034611, https://doi.org/10.1103/PhysRevC.92.034611.

[60] J. Lei, A.M. Moro, Comprehensive analysis of large α yields observed in ^{6}Li-induced reactions, Phys. Rev. C 95 (2017) 044605, https://doi.org/10.1103/PhysRevC.95.044605.

[61] G. Potel, et al., Toward a complete theory for predicting inclusive deuteron breakup away from stability, Eur. Phys. J. A 53 (9) (2017) 178, https://doi.org/10.1140/epja/i2017-12371-9.

[62] T. Nakamura, et al., Coulomb dissociation of a halo nucleus ^{11}Be at 72A MeV, Phys. Lett. B 331 (3) (1994) 296–301, https://doi.org/10.1016/0370-2693(94)91055-3.

[63] K. Ieki, et al., Coulomb dissociation of ^{11}Li, Phys. Rev. Lett. 70 (1993) 730–733, https://doi.org/10.1103/PhysRevLett.70.730.

[64] D. Sackett, et al., Electromagnetic excitation of ^{11}Li, Phys. Rev. C 48 (1993) 118–135, https://doi.org/10.1103/PhysRevC.48.118.

[65] A. Di Pietro, A. Moro, J. Lei, R. de Diego, Insights into the dynamics of breakup of the halo nucleus ^{11}Be on a ^{64}Zn target, Phys. Lett. B 798 (2019) 134954, https://doi.org/10.1016/j.physletb.2019.134954.

[66] F. Duan, et al., Scattering of the halo nucleus 11be from a lead target at 3.5 times the coulomb barrier energy, Phys. Lett. B 811 (2020) 135942, https://doi.org/10.1016/j.physletb.2020.135942.

[67] J. Kolata, et al., Breakup of ^{8}B at sub-Coulomb energies, Phys. Rev. C 63 (2001) 024616, https://doi.org/10.1103/PhysRevC.63.024616.

[68] J.E. Mason, S.B. Gazes, R.B. Roberts, S.G. Teichmann, Coulomb and nuclear effects in direct breakup of 54-MeV ^{7}Li+^{12}C, ^{197}Au, Phys. Rev. C 45 (1992) 2870–2878, https://doi.org/10.1103/PhysRevC.45.2870.

[69] J.A. Tostevin, F.M. Nunes, I.J. Thompson, Calculations of three-body observables in ^{8}B breakup, Phys. Rev. C 63 (2001) 024617, https://doi.org/10.1103/PhysRevC.63.024617.